



OPEN ACCESS

EDITED BY

Ziyu Qin,
Hainan University, China

REVIEWED BY

Hao Dong,
Zhejiang Lab, China
Yangong Zheng,
Ningbo University, China

*CORRESPONDENCE

Hitoshi Tabata,
✉ tabata@bioeng.t.u-tokyo.ac.jp

RECEIVED 20 February 2023

ACCEPTED 20 April 2023

PUBLISHED 02 May 2023

CITATION

Zang C, Zhou H, Ma K, Yano Y, Li S,
Yamahara H, Seki M, Iizuka T and Tabata H
(2023), Electronic nose based on multiple
electrospinning nanofibers sensor array
and application in gas classification.
Front. Sens. 4:1170280.
doi: 10.3389/fsens.2023.1170280

COPYRIGHT

© 2023 Zang, Zhou, Ma, Yano, Li,
Yamahara, Seki, Iizuka and Tabata. This is
an open-access article distributed under
the terms of the [Creative Commons
Attribution License \(CC BY\)](https://creativecommons.org/licenses/by/4.0/). The use,
distribution or reproduction in other
forums is permitted, provided the original
author(s) and the copyright owner(s) are
credited and that the original publication
in this journal is cited, in accordance with
accepted academic practice. No use,
distribution or reproduction is permitted
which does not comply with these terms.

Electronic nose based on multiple electrospinning nanofibers sensor array and application in gas classification

Chuanlai Zang¹, Haolong Zhou¹, Kaijie Ma², Yasuo Yano²,
Shuowei Li¹, Hiroyasu Yamahara¹, Munetoshi Seki¹,
Tetsuya Iizuka¹ and Hitoshi Tabata^{1,2*}

¹Department of Electrical Engineering and Information Systems, Graduate School of Engineering, The University of Tokyo, Tokyo, Japan, ²Department of Bioengineering, Graduate School of Engineering, The University of Tokyo, Tokyo, Japan

To mimic the human olfactory system, an electronic nose (E-nose, also known as artificial olfactory) has been proposed based on a multiple gas sensor array and a pattern recognition algorithm. Detection of volatile organic components (VOCs) has many potential applications in breath analysis, food quality estimation, and indoor and outdoor air quality monitoring, etc. In this study, a facile single-needle electrospinning technology was applied to develop the four different semiconductor metal oxide (MOS) nanofibers sensor arrays (SnO₂, CuO, In₂O₃ and ZnO, respectively). The array shows a smooth surface and constant diameter of nanofiber (average of 150 nm) resulting in high sensitivity to multiple target analyte gases. Five human health related VOCs gases were measured by fabricated E-nose and different response patterns were obtained from four MOS nanofibers sensors. Combined with feature extraction from the response curves, a principal component analysis (PCA) algorithm was applied to reduce the dimension of feature matrix. Thus, the fabricated E-nose system successfully discriminated five different VOCs gases. Real-time and non-invasive gas monitoring by E-nose is very promising for application in human health monitoring, food monitoring, and other fields.

KEYWORDS

metal oxide, gas sensor, sensor array, electronic nose, breath analysis

1 Introduction

Due to their promising ability to detect a wide range of gases, metal oxide gas sensors have been widely used in various fields, such as indoor and outdoor air monitoring (Lee et al., 2021; Zhang et al., 2021), and the food and beverage industry (Li et al., 2019; Abegg et al., 2020; Mohd Ali et al., 2020). However, their poor selectivity limited their use in certain applications. Researchers have attempted to improve the selectivity of metal oxide sensors using various methods such as doping and heterojunction modification (Park et al., 2020). However, the mechanisms underlying these improvements are not completely understood. An alternative approach is to use sensor arrays composed of different metal oxide materials, combined with pattern recognition algorithms to improve selectivity (Liu et al., 2020; Chu et al., 2021). Electronic noses (E-noses) are artificial olfactory systems

that use cross-reactive sensor arrays to generate a fingerprint pattern for target molecules. The development of E-noses has been inspired by the mammalian olfactory system and aims to replicate or even surpass human olfaction (Gao et al., 2021). Since Persaud and Dodd proposed an E-nose for odor classification using chemical sensor array systems in 1982, and the E-nose has attracted considerable attention over past 2 decades. However highly sensitive, intelligent and robust E-nose remains a big challenge. The electronic nose is a kind of gas detection instrument developed to simulate the human olfactory system. Its working process is mainly divided into three steps: first of all, gas sensor arrays often use different semiconductor oxides, two-dimensional materials, or conductive organic substances to obtain different response for different target gas. After the sensor array contacts the target gas molecules, adsorption, reaction and desorption of gas molecules occur on its surface, which changes the electronic properties of the sensor and generates signals. Then, through the sensor analog front-end (AFE) circuit, the generated signal is amplified (Cho et al., 2020), A/D converted, collected and processed, and then transmitted to the computer. Different from the common analysis method, electronic nose detection is not the specific content of a certain component in the experimental sample, but the overall information of volatile components in the sample, which is called “fingerprint” data. Finally, the signal is analyzed by a pattern recognition algorithm to recognize the detected gas molecules.

In recent years, electronic noses (E-noses) have been increasingly utilized for the detection of respiratory gases and human health monitoring (Hsieh and Yao, 2018; Lekha and M, 2021). E-noses consist of arrays of sensors that are able to detect and discriminate a wide range of volatile organic compounds, making them suitable for the detection of respiratory gases. In the field of medical diagnostics, E-noses have been used for the non-invasive monitoring of respiratory gases in order to detect and diagnose diseases. Research has shown that the detection of specific gases such as carbon dioxide, oxygen, and nitric oxide can provide valuable information about the health of the respiratory system and aid in the diagnosis of conditions such as asthma, chronic obstructive pulmonary disease, and pneumonia. Furthermore, E-noses have also been used to detect other gases such as volatile organic compounds which are associated with certain diseases, including but not limited to, lung cancer, tuberculosis and other lung infections. The use of E-noses for the detection of these gases holds the potential to improve patient outcomes and reduce healthcare costs (Park et al., 2019). These devices have proven to be non-invasive, efficient, and cost-effective tools for the diagnosis and management of a wide range of respiratory diseases (Güntner et al., 2016).

In this paper, we presented four nanofibers (SnO₂, CuO, ZnO and In₂O₃, respectively) semiconductor metal oxide electronic nose (MOS E-nose) for respiratory gas diagnosis by facile electrospinning technology. The metal oxide E-nose consists of an array of metal oxide sensors that are sensitive to different gases. Then, the characteristic of the response pattern was extracted by calculating of the transient parameter and a pattern recognition algorithm, which is used to classify the gases based on their fingerprint patterns.

2 Materials and methods

2.1 Materials and instruments

Ethanol, N, N-dimethylformamide (DMF), and Polyvinylpyrrolidone, (PVP; Mw = 1,300,000 g/mol) were purchased from Sigma Aldrich. Tin(II) Chloride Dihydrate (SnCl₂·2H₂O), Copper (II) Chloride Dihydrate (CuCl₂·2H₂O), Zinc Acetate (CH₃COO)₂Zn, Indium (III) Nitrate Trihydrate (In(NO₃)₃·3H₂O) were purchased from FUJIFILM. All chemicals were used as received without further purification. Deionized water was used for all the synthesis processes.

The morphological features of the fabricated nanofibers were analyzed by scanning an electron microscope (SEM, Regulus8230, Hitachi High-Technologies Co., Japan). The oxidation state of the fabricated nanofibers was characterized by X-ray photoelectron spectrometer (XPS, JPS-9010MC, JEOL, Japan) and the chemical composition and distribution were evaluated by energy dispersive spectroscopy (EDS, Inca Energy for JSM, JEOL, Japan).

2.2 Fabrication of the SnO₂-CuO nanowires gas sensor

First, the original silicon wafer substrate had a 525 μm-thick (1 0 0) p-type silicon layer and was covered by a 100 μm-thick top layer acting as an insulator. The wafer dicing process is performed by a silicon stealth dicing machine (DFL7340, DISCO, Japan). For the gas sensing measurements, Pt interdigital electrodes with ~100 nm thickness were deposited on the substrate by the traditional lift-off process by laser lithography and sputtering (S-QAM, ULVAC Inc., Japan). To prepare the electrospinning precursor solution, 0.45 g of SnCl₂·2H₂O, 3.4 g of CuCl₂·2H₂O, 0.366 g, (CH₃COO)₂Zn and 0.71 g In(NO₃)₃·3H₂O were separately dissolved in a mixed solution of 5 mL ethanol and 5 mL DMF under stirring for 1 h at room temperature until the powder was completely dissolved. Then, 1 g of PVP was slowly added into the above solution under stirring for 3 h at 50 °C until a viscous precursor solution was formed. The electrospinning machine was purchased from Fuce Co., Ltd. (Japan). The prepared precursor solution was loaded into a glass syringe, with a stainless-steel needle. The electrospinning experiments were performed at a flow rate of 5 mL/min under an applied voltage of 25 kV with a distance of 20 cm from the needle tip collector for 1 h. The schematic diagram of the electrospinning process is shown in Figure 1. During the electrospinning process, copper tape was used to protect the contact pin of electrode during electrospinning process. The as-spun nanofibers were placed in a programmable furnace and raised the temperature to 500 °C within 2 h and calcined at 500 °C for 2 h (Song et al., 2022; Chen et al., 2023). The electronic connection of the sensor chip and ceramic dual inline package (DIP) was performed by a manual wire bonder (7476D, WestBond Inc., Japan).

2.3 Measurement of gas sensing proprieties

The gas sensing tests were carried out with a homemade setup based on a test chamber with a test probe inside and a Keithley

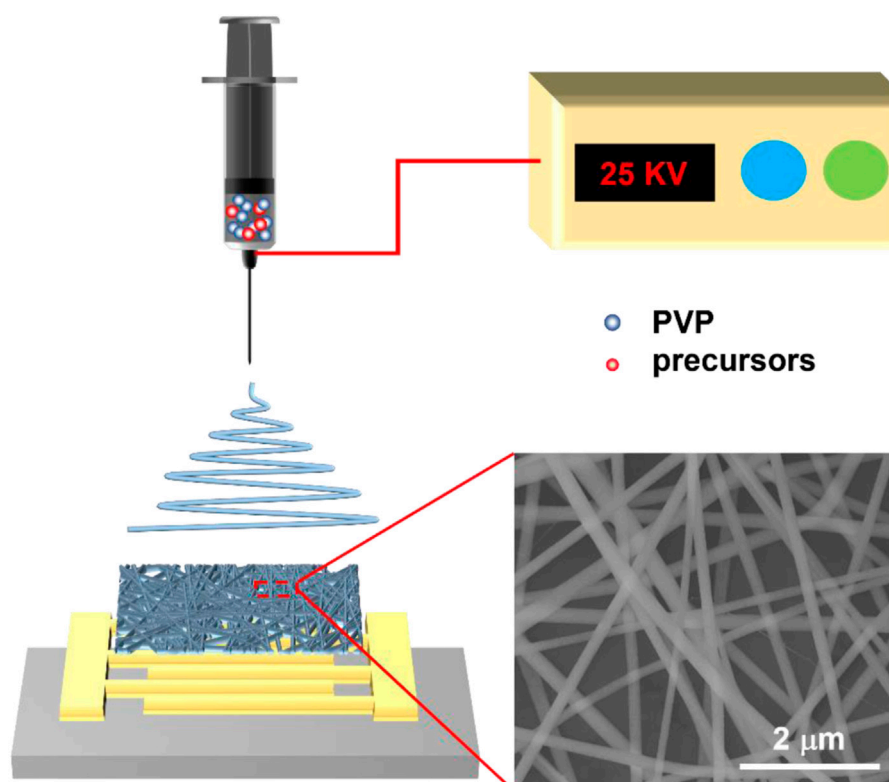


FIGURE 1
Schematic diagram of the electrospinning process and electron microscope image of as-spun nanofibers.

4200A-SCS semiconductor analyzer. The Keithley applied a steady DC voltage of 1 V and the resistance was calculated by recording the current. The concentration of test gas was controlled by the amount of gas injection. The operating temperature was controlled at 300 °C using a heating plate by applying different DC voltages. The response of the gas sensor was defined by the equation response $(R) = R_a/R_g$ for n-type metal oxide gas sensors and $R = R_g/R_a$ for p-type metal oxide gas sensors, where R_a and R_g are the electrical resistance of the sensor under air and target gas atmosphere, respectively.

3 Results and discussion

3.1 Morphological characterizations of four nanofibers gas sensor array

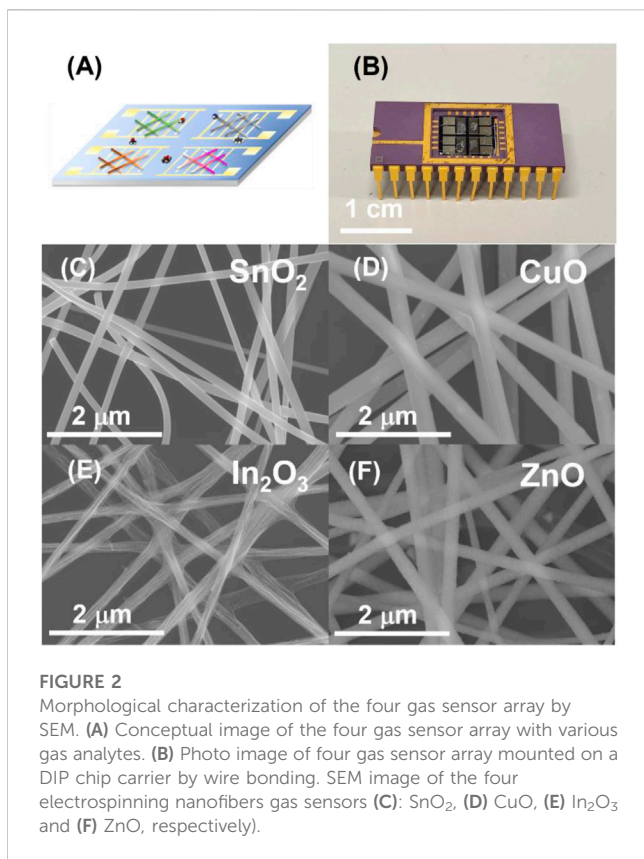
A schematic illustration of the fabrication of a gas sensor array based E-nose chip by general single-needle electrospinning technology was shown in Figure 2A. Four Pt interdigital electrodes were deposited by traditional lift-off process via laser lithography and sputtering on the SiO₂/Si substrate. Furthermore, four MOS (SnO₂, CuO, In₂O₃ and ZnO) nanofibers sensing material were deposited on the interdigital electrodes by facile single-needle electrospinning technology followed by a calcination process to remove PVP and oxidation (Wang et al., 2016). Finally, the E-nose chip was loaded on a ceramic dual inline package by wire

bonding and the optical image is shown in Figure 2B. These four semiconductor metal oxides were always the popular choice for E-nose and their typical physical and chemical property is listed in Table 1.

Scanning electron microscopy (SEM) images were used to analyze the electrospinning nanofibers of four different metal oxides. The SEM image of four MOS nanofibers is shown in Figures 2E,F. The diameter of the as-spun electrospinning nanofibers contained PVP and metal elements. The nanofibers were randomly distributed in the wafer substrate, which formed a multichannel conduction channel between integrated digital electrodes. Different MOS nanofibers were demonstrated to be a homogeneous structures with an approximately similar diameter (≈ 150 nm). From the SEM result, high diameter uniformity, high density of nanofibers, and surface smoothness guarantee the stability and sensitivity of the fabricated nanofibers for use in gas sensing. The large high specific surface area also leads to high sensitivity of the nanofiber-based gas sensor (Mirzaei et al., 2019).

3.2 EDS and XPS characterization

SEM and energy dispersive X-ray spectroscopy (EDS) mapping of the nanofibers were conducted to investigate the morphology, elemental composition and distribution of the four MOS nanofibers gas sensor arrays (Figures 3A–H). The results indicated that the four semiconductor metal oxide nanofibers (CuO, In₂O₃, SnO₂, and



ZnO) were successfully fabricated. Additionally, the EDS mapping analysis was also used to investigate the distribution of elements within the nanowires. From the EDS mapping result, four types of elements (Sn, Cu, Zn and In) were uniformly distributed throughout the nanofibers, indicating that the synthesis process had been successful in fabricating homogenous nanowires.

To precisely confirm the oxidation states and elemental chemistries of the four gas sensor arrays, X-ray photoelectron spectroscopy (XPS) analysis was conducted and discussed below (Figures 3I–L). Figure 3I, two peaks are clearly observed in the SnO₂ XPS analysis. Two characteristic peaks centered at 495.3 (3d_{3/2}) eV and 486.9 (3d_{5/2}) eV, respectively, which are attributed to the Sn⁴⁺ state. The tin chloride precursor was transformed into Sn⁴⁺ phases, rather than Sn²⁺ phases during the thermal calcination oxidation process. In the XPS spectrum of the CuO channel shown in Figure 3J, two characteristic peaks for 2p_{1/2} and 2p_{3/2} were observed at a binding energy of 953.7 eV and

933.76 eV, respectively, corresponding to the binding energy of Cu²⁺. This result indicates that the copper chloride precursor is transformed into CuO phases, rather than Cu₂O phases during the thermal calcination oxidation process. In the survey of the In₂O₃ spectrum (Figure 3K), two characteristic peaks for and were shown at a binding energy of 453.1 eV and 445.5 eV, respectively, corresponding to In³⁺. The oxidation state of the ZnO nanofibers was clearly shown in Figure 3L. Two characteristic peaks in the XPS analysis at 1021.6 eV and 1044.8 eV. Overall, the XPS results clearly demonstrated the oxidation state of four different MOS nanofibers.

3.3 Gas sensing response of the four MOS nanofibers gas sensor array

The gas sensing responses of the fabricated gas sensor were measured toward five kinds of target VOCs analyte gases (ammonia, ethanol, acetaldehyde, isoprene and acetone). These five gases were selected for measurement mainly because each gas is closely related to human health and disease. For example, ammonia has been proven to be closely related to body fatigue and hepatitis. Isoprene is commonly used to identify the blood cholesterol level. Acetaldehyde is a well-known biomarker for lung cancer. Moreover, acetone is well known to be associated with fat burning and diet. Ethanol is a well-known detection target to represent the alcohol drinking level. Some typical properties of selected gases are listed in Table 2. These health marks VOCs gases exhaled from human breath and skin from ppb to ppm order. So, the smart electronic nose should have the ability to detect these five VOCs analyte gases in ppb to ppm level and discriminated them from interfering gases. Since the exhaled gases contain a large concentration of water vapor, the effect of humidity should also be quantitatively evaluated in the future (Tai et al., 2020; Dong et al., 2022). The practical applications of gas sensors are determined by their sensitivity, stability, and selectivity. However, it is unclear whether the fabricated gas sensor can produce a stable response to minute changes in the gas concentration, as well as whether the sensor array can specifically identify different gas components. These aspects should be studied in detail in the future (Sanchez et al., 2019).

Here, these five VOCs analyte gases were tested together by fabricated MOS E-nose and distinguished with the combination with PCA algorithm (Khan et al., 2020). The concentrations of five kinds of VOCs analyte gases were set to 20 ppm. The analytes were

TABLE 1 The physical and chemical properties of semiconductor metal oxide (Iwamoto et al., 1978; Zhai et al., 2009).

| | SnO ₂ | ZnO | In ₂ O ₃ | CuO |
|--|-------------------------|-------------------------|--------------------------------|-------------------------|
| Type | N-type | N-type | N-type | P-type |
| Crystal structures | Tetragonal | Hexagonal | Cubic | Cubic |
| Band gap (eV) | 3.6 | 3.37 | 3.6 (direct) | 1.4 |
| | | | 2.5 (indirect) | |
| Oxygen desorption amount (STP/m ²) | 2.11 × 10 ⁻³ | 2.45 × 10 ⁻⁴ | 4.37 × 10 ⁻³ | 1.42 × 10 ⁻¹ |

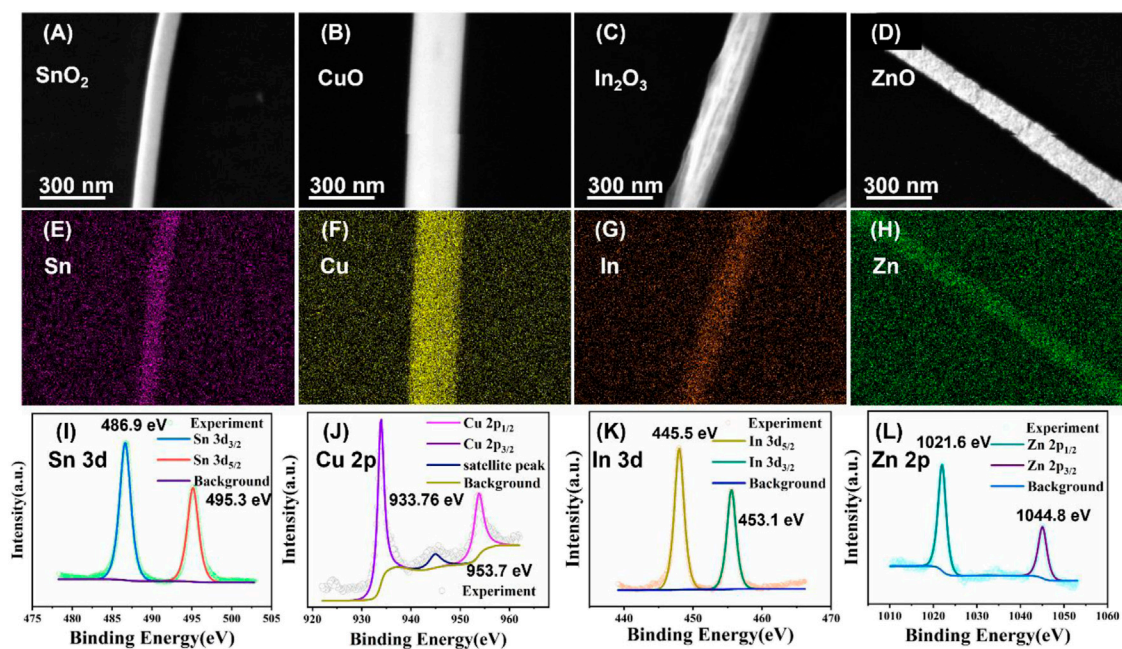


FIGURE 3

Magnified SEM image of the four nanofibers (A) SnO₂, (B) CuO, (C) In₂O₃, and (D) ZnO gas sensor. EDS mapping of four nanofibers (E) SnO₂, (F) CuO, (G) In₂O₃, and (H) ZnO gas sensor. XPS spectra of four nanofibers (I) SnO₂, (J) CuO, (K) In₂O₃, and (L) ZnO gas sensor.

TABLE 2 Summary of typical VOCs and their related symptoms (Menezes et al., 2013; Belizario et al., 2021).

| | Molecular size (Å) | Molecular weight (g/mol) | Concentration (ppb/min) | Dipole moment | Related symptoms |
|--------------|--------------------|--------------------------|-------------------------|---------------|-----------------------------|
| Ammonia | 2.3 | 17.07 | 0.3–8 | 1.48D | Fatigue, hepatitis |
| Isoprene | 4.7 | 68.12 | 1.6–10.3 | 0.29 D | blood cholesterol |
| Acetaldehyde | 3.8 | 44.05 | 0.9–23 | 2.7D | Lung cancer, hangover |
| Acetone | 4.6 | 58.08 | 2.8–27 | 2.8D | Fat burning, diet, diabetes |
| Ethanol | 4.3 | 46.07 | 3.6–246 | 1.6D | Drinking level |

injected into a homemade gas testing chamber in series. The resistances of the channels were tested using probe station, and the variations of the electrical resistances of the four MOS nanofibers gas sensors were recorded by Keithley 4200A-SCS semiconductor analyzer. The testing temperature was set at 300 °C.

The response of each gas sensor toward various target VOCs analytes was defined by the equation $\text{response} = R_a/R_g$ for n-type MOS (SnO₂, In₂O₃ and ZnO) gas sensor, and $\text{response} = R_g/R_a$ for p-type MOS (CuO) gas sensor for further PCA analysis. Here, R_a represents the base electrical resistance (baseline) of the sensor under air atmosphere, and R_g represents the electrical resistance that occurs when the target VOCs analytes gases were introduced. The definition of response is different due to the different sensing mechanisms of n-type and p-type semiconductors, such as different main charge carriers and different charge transport pathways (Kang et al., 2020). For example, the SnO₂ nanofibers gas sensor showed gas response values ranging from 3.4 (acetaldehyde) to 23.8 (ethanol) (Figure 4A). Ethanol showed

relatively active properties among all four types of metal oxide semiconductors, and isoprene and acetaldehyde showed relatively inactive properties among all four kinds of metal oxide semiconductors. The p-type metal oxide semiconductor CuO channel provided relatively low response sensitivity compared with the other channels. These low response sensitivities was due to the electrical properties and the sensing mechanism of p-type metal oxide semiconductors (Lupan et al., 2016). Figure 4F shows the standardized fingerprint of four sensor arrays for five different gases. The standardization method is simple: the response of each gas is divided by the maximum response obtained among the five gases. This helps to normalize the data and make it easier to compare the responses of the four sensors to each gas. The fingerprint shows the unique patterns of the four sensor arrays and highlights the specific gas-sensing properties of each one, providing a comprehensive overview of the performance of the sensors in detecting different gases, making it a useful tool for evaluating the efficiency and effectiveness of the sensor arrays.

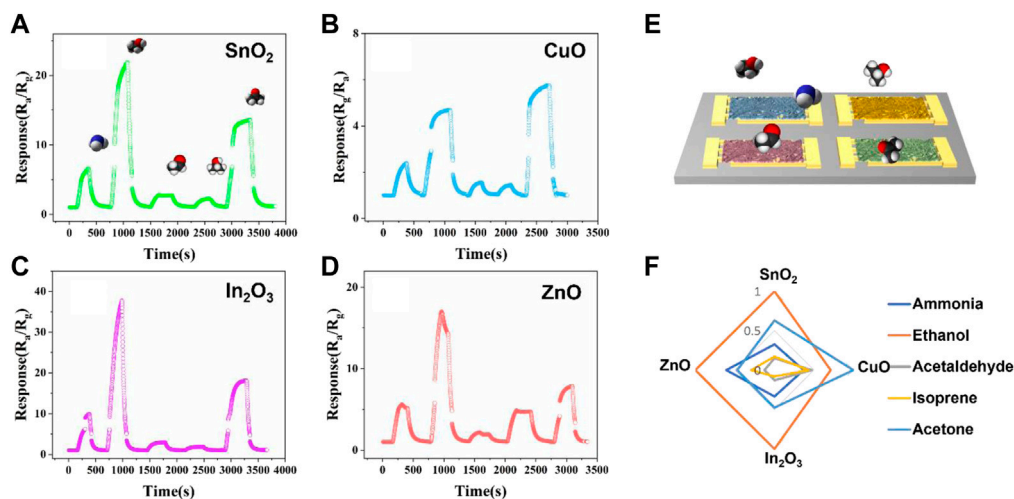


FIGURE 4

Sensing performance of the fabricated four types of nanofibers (A) SnO_2 , (B) CuO , (C) In_2O_3 and (D) ZnO MOS gas sensor array to five different target gases (from left to right: 20 ppm samples of ammonia, ethanol, acetaldehyde, isoprene and acetone were introduced in series). (E) Diagram of fabricated nanofibers gas sensor array E-nose. (F) Standardized fingerprint response of the four-channel nanofibers electronic nose.

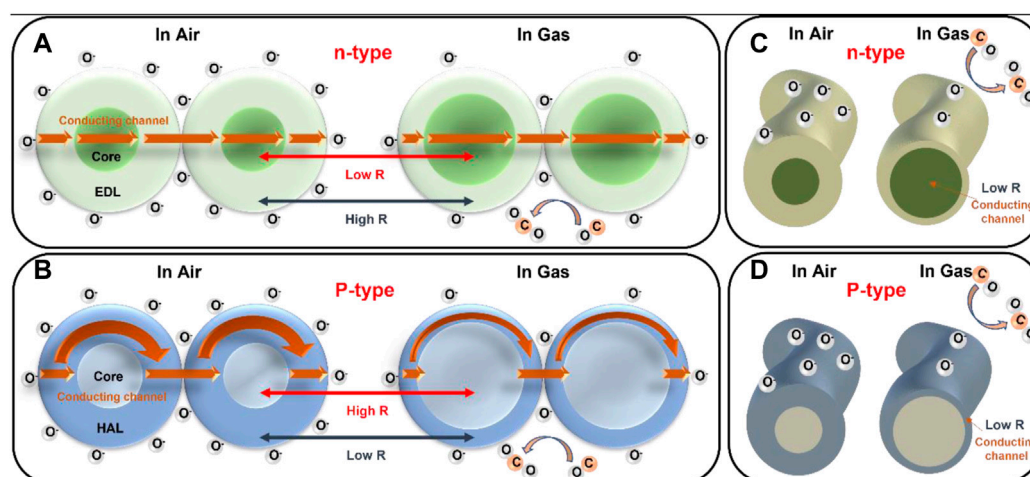


FIGURE 5

Schematic diagram of gas sensing mechanism and conduction model for (A) n-type MOS particle model, (B) p-type MOS particle model, (C) n-type MOS nanowire model, (D) p-type MOS nanowire model.

3.4 Mechanism analysis

The mechanism of MOS gas sensing is summarized in Figure 5. The detection of gas molecules is based on the electrical conductivity of an oxide semiconductor changes in response to the adsorption of gas molecules. Figure 5A and 5B shows the particle model for n-type and p-type MOS, and Figures 5C, D show the nanowire model for n-type and p-type MOS. In the n-type oxide semiconductors, the adsorption of oxygen and its ionization to O^{2-} , O^- , and O^{2-} at temperatures ranging from 100°C to 450°C creates the core-shell electronic configuration. The core is semiconducting while the shell is a resistive electron depletion layer (EDL). For particles larger than

twice thickness of the EDL, the electron must overcome the Schottky barrier at the grain boundary. Thus, conduction is explained by the serial connection between the semiconducting cores and the resistive shells. In contrast, p-type oxide semiconductors have a different electronic configuration, with the ionized oxygen on the surface attracting the majority of charge carriers (holes) to form the core-shell structure. The core is less conductive, while the shell is a semiconducting hole accumulation layer (HAL). For particle diameters larger than twice thickness of the HAL, conduction is determined by the parallel competition between two pathways, one through the semiconducting HAL with the narrower cross-sectional area and the other through the less conductive core with the wider

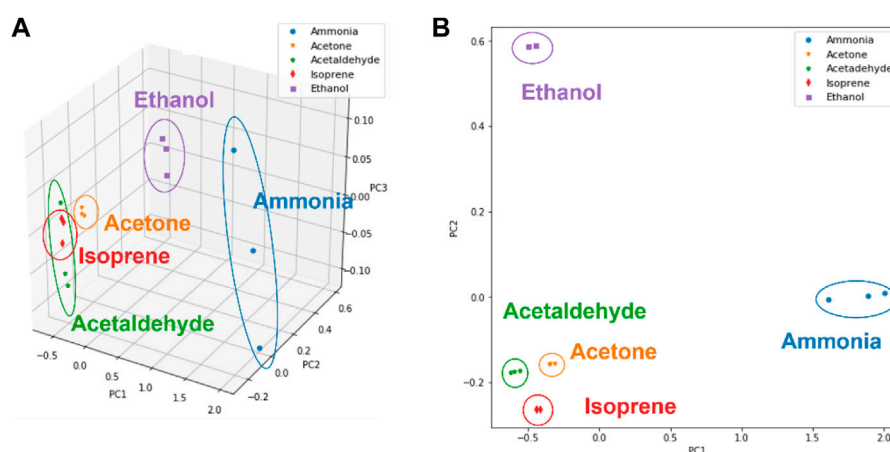


FIGURE 6

Gases recognition for five kinds of VOCs (ammonia, ethanol isoprene, acetaldehyde, isoprene and acetone) by PCA algorithm. (A) 3D PCA result. (B) 2D PCA result.

cross-sectional area. When electrons are injected into the sensing materials due to the reaction between ionized oxygen and the reducing gas, the electron concentration in the EDL increases in n-type chemiresistors, while the hole concentration in the HAL decreases in p-type chemiresistors, resulting in opposite chemiresistive variations. Therefore, n-type oxide semiconductors with serial conduction paths are more advantageous for achieving higher sensor resistance variations than p-type semiconductors with parallel conduction paths.

3.5 PCA pattern analysis

To investigate the gas classification performance of the fabricated multiple nanofibers array E-nose system, pattern recognition analysis was conducted by PCA analysis to distinguish between the five different target VOCs analyte gases. First, feature extraction was calculated from the response curve for the following PCA analysis (Yan and Zhang, 2015). In this work, these four features were calculated based dynamic process of surface gas sensing, which includes gas adsorption, reaction, and recovery. ΔR is defined as the difference value of the maximum resistance and the baseline resistance. $|\Delta R|$ is calculated as a normalized version of resistance change by calculating the division of resistance change ΔR and baseline resistance. Moreover, the adsorption and recovery process also provide meaningful features to distinguish different target gases. The response time during adsorption is defined as the time required for a sensor to reach 90% of the total response of the signal upon exposure to the target gas. Recovery time is calculated as the time required for a sensor to return to 90% of the original baseline signal upon removal of the target gas. The extracted 16-dimensional database was then applied to PCA algorithms to reduce the dimensionality of the database into two-dimension and three-dimension. The result was shown in Figures 6A, B, combined with fabricated nanofibers E-nose and PCA algorithm five kinds of gas can be clearly distinguished after being applied PCA algorithm.

4 Conclusion

In this study, a high-performance four MOS nanofibers E-nose system was developed by a facile electrospinning technology. Four different semiconductor metal oxide (MOS) nanofibers sensor arrays (SnO_2 , CuO, In_2O_3 and ZnO, respectively) exhibited smooth surfaces and constant diameter of nanofibers (an average of 150 nm) resulting in high sensitivity toward the multiple target analyte gases. Five kinds of human health-related target VOCs analyte gases (ammonia, ethanol, acetaldehyde, isoprene and acetone) were measured by the fabricated MOS E-nose and different response patterns were obtained by four MOS nanofibers gas sensors. The feature of different response patterns was extracted and applied to PCA algorithm. It was found that five kinds of target gases were successfully identified. Furthermore, the demonstration of breath detection also revealed the potential application in real-time and non-invasive breath analysis and health monitoring.

Data availability statement

The raw data supporting the conclusion of this article will be made available by the authors, without undue reservation.

Author contributions

CZ carried out the experiment with support from YY. CZ wrote the manuscript with support from HZ, KM, HY, MS. SL, and TI fabricated the chip package and multiple gases test. HT supervised the project and instructed the manuscript writing. All authors contributed to the article and approved the submitted version.

Funding

This research was partially supported by AMED under Grant Number JP222zf0127006, JSPS KAKENHI Grant Number

JP20H05651, and Institute for AI and Beyond for the University of Tokyo. This work was also partially supported by the Graduate Program for International Graduate Program of Innovation for Intelligent World (IIW) of The University of Tokyo by MEXT (Ministry of Education, Culture, Sports, Science and Technology).

Acknowledgments

The authors would like to express their gratitude to Professor Tomoyuki Yokota and Dr. Chihiro Okutani for their guidance of instruments and valuable suggestions.

References

- Abegg, S., Magro, L., van den Broek, J., Pratsinis, S. E., and Güntner, A. T. (2020). A pocket-sized device enables detection of methanol adulteration in alcoholic beverages. *Nat. Food* 1 (6), 351–354. doi:10.1038/s43016-020-0095-9
- Belizario, J. E., Faintuch, J., and Malpartida, M. G. (2021). Breath biopsy and discovery of exclusive volatile organic compounds for diagnosis of infectious diseases. *Front. Cell. Infect. Microbiol.* 10, 564194. doi:10.3389/fcimb.2020.564194
- Chen, L., Shi, H. Z., Ye, C. J., Xia, X. Y., Li, Y., Pan, C. Y., et al. (2023). Enhanced ethanol-sensing characteristics of Au decorated In-doped SnO₂ porous nanotubes at low working temperature. *Sensors Actuators B-Chemical* 375, 132864. doi:10.1016/j.snb.2022.132864
- Cho, S. Y., Lee, Y., Lee, S., Kang, H., Kim, J., Choi, J., et al. (2020). Finding hidden signals in chemical sensors using deep learning. *Anal. Chem.* 92 (9), 6529–6537. doi:10.1021/acs.analchem.0c00137
- Chu, J., Li, W., Yang, X., Wu, Y., Wang, D., Yang, A., et al. (2021). Identification of gas mixtures via sensor array combining with neural networks. *Sensors Actuators B Chem.* 329, 129090. doi:10.1016/j.snb.2020.129090
- Dong, H., Qian, L. B., Cui, Y. X., Zheng, X. B., Cheng, C., Cao, Q. P., et al. (2022). Online accurate detection of breath acetone using metal oxide semiconductor gas sensor and diffusive gas separation. *Front. Bioeng. Biotechnol.* 10, 861950. doi:10.3389/fbioe.2022.861950
- Gao, Z., Chen, S., Li, R., Lou, Z., Han, W., Jiang, K., et al. (2021). An artificial olfactory system with sensing, memory and self-protection capabilities. *Nano Energy* 86. doi:10.1016/j.nanoen.2021.106078
- Güntner, A. T., Koren, V., Chikadi, K., Righettoni, M., and Pratsinis, S. E. (2016). E-nose sensing of low-ppb formaldehyde in gas mixtures at high relative humidity for breath screening of lung cancer? *ACS Sensors* 1 (5), 528–535. doi:10.1021/acssensors.6b00008
- Hsieh, Y.-C., and Yao, D.-J. (2018). Intelligent gas-sensing systems and their applications. *J. Micromechanics Microengineering* 28 (9), 093001. doi:10.1088/1361-6439/aac849
- Iwamoto, M., Yoda, Y., Yamazoe, N., and Seiyama, T. (1978). Study of metal-oxide catalysts by temperature programmed desorption. 4. Oxygen-adsorption on various metal-oxides. *J. Phys. Chem.* 82 (24), 2564–2570. doi:10.1021/j100513a006
- Kang, H., Cho, S. Y., Ryu, J., Choi, J., Ahn, H., Joo, H., et al. (2020). Multiarray nanopattern electronic nose (E-Nose) by high-resolution top-down nanolithography. *Adv. Funct. Mater.* 30 (27), 2002486. doi:10.1002/adfm.202002486
- Khan, M. A. H., Thomson, B., Debnath, R., Motayed, A., and Rao, M. V. (2020). Nanowire-based sensor array for detection of cross-sensitive gases using PCA and machine learning algorithms. *IEEE Sensors J.* 20 (11), 6020–6028. doi:10.1109/jsen.2020.2972542
- Lee, J., Jung, Y., Sung, S.-H., Lee, G., Kim, J., Seong, J., et al. (2021). High-performance gas sensor array for indoor air quality monitoring: The role of Au nanoparticles on WO₃, SnO₂, and NiO-based gas sensors. *J. Mater. Chem. A* 9 (2), 1159–1167. doi:10.1039/d0ta08743b
- Lekha, S., and Suchetha, M. (2021). Recent advancements and future prospects on E-nose sensors technology and machine learning approaches for non-invasive diabetes diagnosis: A review. *IEEE Rev. Biomed. Eng.* 14, 127–138. doi:10.1109/RBME.2020.2993591
- Li, Z., Paul, R., Ba Tis, T., Saville, A. C., Hansel, J. C., Yu, T., et al. (2019). Non-invasive plant disease diagnostics enabled by smartphone-based fingerprinting of leaf volatiles. *Nat. Plants* 5 (8), 856–866. doi:10.1038/s41477-019-0476-y
- Liu, H., Meng, G., Deng, Z., Li, M., Chang, J., Dai, T., et al. (2020). Progress in research on VOC molecule recognition by semiconductor sensors. *Acta Phys. Chim. Sin.* 38 (5), 2008018. doi:10.3866/pku.Whxb202008018
- Lupan, O., Postica, V., Cretu, V., Wolff, N., Duppel, V., Kienle, L., et al. (2016). Single and networked CuO nanowires for highly sensitive p-type semiconductor gas sensor applications. *Phys. status solidi (RRL) - Rapid Res. Lett.* 10 (3), 260–266. doi:10.1002/psr.201510414
- Menezes, H. C., Amorim, L. C. A., and Cardeal, Z. L. (2013). Sampling and analytical methods for determining VOC in air by biomonitoring human exposure. *Crit. Rev. Environ. Sci. Technol.* 43 (1), 1–39. doi:10.1080/10643389.2011.604239
- Mirzaei, A., Lee, J.-H., Majhi, S. M., Weber, M., Bechelany, M., Kim, H. W., et al. (2019). Resistive gas sensors based on metal-oxide nanowires. *J. Appl. Phys.* 126 (24), 241102. doi:10.1063/1.5118805
- Mohd Ali, M., Hashim, N., Abd Aziz, S., and Lasekan, O. (2020). Principles and recent advances in electronic nose for quality inspection of agricultural and food products. *Trends Food Sci. Technol.* 99, 1–10. doi:10.1016/j.tifs.2020.02.028
- Park, K.-R., Cho, H.-B., Lee, J., Song, Y., Kim, W.-B., and Choa, Y.-H. (2020). Design of highly porous SnO₂-CuO nanotubes for enhancing H₂S gas sensor performance. *Sensors Actuators B Chem.* 302, 127179. doi:10.1016/j.snb.2019.127179
- Park, S. Y., Kim, Y., Kim, T., Eom, T. H., Kim, S. Y., and Jang, H. W. (2019). Chemoresistive materials for electronic nose: Progress, perspectives, and challenges. *InfoMat* 1 (3), 289–316. doi:10.1002/inf2.12029
- Sanchez, C., Santos, J. P., and Lozano, J. (2019). Use of electronic noses for diagnosis of digestive and respiratory diseases through the breath. *Biosens. (Basel)* 9 (1), 35. doi:10.3390/bios9010035
- Song, Y. H., Dong, H., Liu, W. X., Fu, X., Fu, Z., Li, P. L., et al. (2022). Electrostatic jet engineering of flexible composite pressure sensors for physical applications. *ACS Appl. Polym. Mater.* 4 (2), 868–878. doi:10.1021/acscpm.1c01357
- Tai, H., Wang, S., Duan, Z., and Jiang, Y. (2020). Evolution of breath analysis based on humidity and gas sensors: Potential and challenges. *Sensors Actuators B Chem.* 318, 128104. doi:10.1016/j.snb.2020.128104
- Wang, Y., Zhang, H., and Sun, X. (2016). Electrospun nanowires of NiO/SnO₂ p-n heterojunctions for enhanced gas sensing. *Appl. Surf. Sci.* 389, 514–520. doi:10.1016/j.apsusc.2016.07.073
- Yan, K., and Zhang, D. (2015). Feature selection and analysis on correlated gas sensor data with recursive feature elimination. *Sensors Actuators B Chem.* 212, 353–363. doi:10.1016/j.snb.2015.02.025
- Zhai, T. Y., Fang, X. S., Liao, M. Y., Xu, X. J., Zeng, H. B., Yoshio, B., et al. (2009). A comprehensive review of one-dimensional metal-oxide nanostructure photodetectors. *Sensors* 9 (8), 6504–6529. doi:10.3390/s90806504
- Zhang, J., Xue, Y., Sun, Q., Zhang, T., Chen, Y., Yu, W., et al. (2021). A miniaturized electronic nose with artificial neural network for anti-interference detection of mixed indoor hazardous gases. *Sensors Actuators B Chem.* 326, 128822. doi:10.1016/j.snb.2020.128822

Conflict of interest

The authors declare that the research was conducted in the absence of any commercial or financial relationships that could be construed as a potential conflict of interest.

Publisher's note

All claims expressed in this article are solely those of the authors and do not necessarily represent those of their affiliated organizations, or those of the publisher, the editors and the reviewers. Any product that may be evaluated in this article, or claim that may be made by its manufacturer, is not guaranteed or endorsed by the publisher.